Journal of Zhejiang University-SCIENCE B 2026 27(9):1013-1030
www.jzus.zju.edu.cn; www.springer.com/journal/11585
E-mail: jzus_b@zju.edu.cn

Research Article
https://doi.org/10.1631/jzus.B2500216

Check for updates

Reduced nerve growth factor (NGF) mediates arsenic-induced mitochondrial dynamics imbalance and neuronal damage both in vivo and in vitro

Xinbo MA[1,2,3,4], Liu YANG[1,3,4], Xinhua SHAO[1,3,4], Jia CUI[1,3,4], Ziqiao GUAN[1,3,4], Man LYU[1,3,4], Shuaifei YANG[1,3,4], Na FANG[1,3,4], Yang LIU[1,3,4], Yanhui GAO[1,3,4], Xiaona LIU[1,3,4]✉, Yanmei YANG[1,3,4]✉

[1]*Center for Endemic Disease Control, Chinese Center for Disease Control and Prevention, Harbin Medical University, Harbin 150081, China*
[2]*Xi'an Center for Disease Control and Prevention, Xi'an 710000, China*
[3]*NHC Key Laboratory of Etiology and Epidemiology (Harbin Medical University), Harbin 150081, China*
[4]*Joint Key Laboratory of Endemic Diseases (Harbin Medical University, Guizhou Medical University, Xi'an Jiaotong University), Harbin 150081, China*

Abstract: Arsenic exposure is known to cause cognitive deficits, although the underlying mechanisms are yet to be explored. In this study, we investigated the role of nerve growth factor (NGF), a neuroprotective factor, in arsenic-induced cognitive impairment. In mouse models exposed to 25 and 50 mg/L sodium arsenite ($NaAsO_2$), we observed neuronal damage accompanied by the downregulation of NGF, decreased phosphorylation of phosphatidylinositol 3-kinase/protein kinase B (PI3K/AKT), reduced phosphorylation of the mitochondrial fission protein dynamin-related protein 1 (Drp1), and downregulation of the mitochondrial fusion protein optic atrophy 1 (OPA1). Similarly, the downregulation of NGF, inactivation of the PI3K/AKT signaling pathway, mitochondrial dynamics imbalance (dysregulation of mitochondrial fission and fusion processes), and increased apoptosis were observed in HT-22 cells exposed to 4 μmol/L $NaAsO_2$. NGF overexpression mitigated these arsenic-induced alterations, while the protective effect of NGF against arsenic toxicity was reduced by LY294002, a PI3K/AKT pathway inhibitor. These findings suggest that a decrease in NGF mediates the arsenic-disrupted mitochondrial dynamics via inhibiting the PI3K/AKT pathway, ultimately impairing cognitive function.

Key words: Arsenic; Nerve growth factor (NGF); Mitochondrial dynamics; Neurotoxicity; Phosphatidylinositol 3-kinase/protein kinase B (PI3K/AKT)

1 Introduction

Arsenic, a naturally occurring toxic metalloid, primarily enters the human body through contaminated water, food, soil, and atmospheric deposition (Sevak and Pushkar, 2024; Xing et al., 2024). Globally, more than 200 million people consume drinking water with arsenic levels exceeding 10 μg/L—the maximum limit set by the World Health Organization (WHO)—making arsenic exposure a significant public health concern (Bozack et al., 2019; Peel et al., 2022). Epidemiological studies have reported significant reductions in verbal intelligence quotient (IQ), spatial memory, and long-term memory in children chronically exposed to arsenic concentrations above 10 μg/L in drinking water (Hong et al., 2014; Liu and Bain, 2018). A cross-sectional study including 1556 adults in China identified a negative correlation between hair arsenic levels and Mini-Mental State Examination (MMSE) scores, suggesting that arsenic may be an independent risk factor for cognitive impairment (Wang et al., 2021). Moreover, exposure to drinking water containing 100 μg/L arsenic for two weeks severely impaired the spatial and contextual memory of mice (Cronican et al., 2013). These observations indicate that prolonged arsenic exposure is positively associated with cognitive impairment; however, the specific mechanisms underlying this damage remain unclear.

Arsenic has been reported to exert toxic effects on brain mitochondria (Prakash et al., 2016). Mitochondria

✉ Xiaona LIU, xiaonaliu_2013@163.com
Yanmei YANG, yangyanmei@hrbmu.edu.cn
Xiaona LIU, https://orcid.org/0000-0002-9856-0801
Yanmei YANG, https://orcid.org/0000-0001-9531-4253

Received Apr. 28, 2025; Revision accepted Aug. 11, 2025; Crosschecked July 10, 2026; Published online Aug. 6, 2026

© Zhejiang University Press 2026

are highly dynamic organelles that undergo continuous fission and fusion processes, collectively known as mitochondrial dynamics, to maintain normal function (Fei et al., 2019; Mu et al., 2019). The balance of mitochondrial dynamics is crucial for neuronal development, plasticity, and function, while an imbalance thereof can lead to mitochondrial dysfunction, disrupted neuronal activity, cognitive impairment, and other neurodegenerative conditions (Bertholet et al., 2016; Chen et al., 2023). The regulation of mitochondrial dynamics involves multiple regulatory proteins, including dynamin-related protein 1 (Drp1) and mitochondrial fission protein 1 (Fis1), which mediate mitochondrial fission, as well as optic atrophy 1 (OPA1) and mitochondrial fusion protein 1/2 (Mfn1/2), which mediate mitochondrial fusion (Yapa et al., 2021). A decrease in Drp1 reduced the number of forebrain synapses and impaired the development of primary neuronal cells in mice, while a deficiency in OPA1 induced neuronal apoptosis and mitochondrial dysfunction (Olichon et al., 2003; Ishihara et al., 2009). Drp1 phosphorylation at Ser616 plays an important role in regulating mitochondrial fission and neurodevelopment, and the phosphorylation status of Ser616 directly affects mitochondrial dynamic balance (Gao et al., 2022). Research indicates that arsenic can impair mitochondrial function by causing excessive mitochondrial fission in myocardial cells, leading to irreversible damage to myocardial differentiation and embryonic development (Jeong et al., 2023). In addition, arsenic toxicity in testes and germ cells has been linked to the disruption of mitochondrial fusion and fission (Ye et al., 2023). Related research has shown that arsenic exposure leads to a significant decrease in the phosphorylation levels of phosphatidylinositol 3-kinase (PI3K), protein kinase B (AKT) and AKT's downstream mammalian target of rapamycin (mTOR), thereby relieving the inhibition of autophagy, eventually inducing ferroptosis and autophagic cell death, and that this pathway inhibition will also disrupt mitochondrial dynamic balance (Liu et al., 2020; Lu HM et al., 2023, 2024). However, the precise mechanisms by which arsenic disrupts mitochondrial dynamics remain unclear, particularly regarding the key regulatory proteins involved in this process.

Nerve growth factor (NGF), the first identified neuroprotective regulator within the neurotrophic factor family (Baruch-Eliyahu et al., 2019), plays a crucial role in neurogenesis and nerve regeneration by regulating mitochondrial dynamics, reorganizing mitochondrial networks, and maintaining mitochondrial mass, membrane potential, and bioenergetic capacity (Martorana et al., 2018). Specifically, NGF enhances mitochondrial fission and fusion by increasing phosphorylated Drp1 (p-Drp1) and OPA1 levels, respectively, leading to alterations in the mitochondrial length and density, thereby maintaining neurons in a highly active state to accommodate the energy requirements of normal neuronal growth (Martorana et al., 2018). NGF exerts dual biological functions—promoting neuronal trophism and adaptive growth—and plays a critical regulatory role in the survival, development, function, and plasticity of central neurons (Sung et al., 2018; Cho et al., 2020). NGF binds to its receptor tyrosine kinase A (TrkA) and exerts neuroprotective effects by activating downstream signaling molecules such as phosphorylated PI3K/AKT (Marlin and Li, 2015; Yan et al., 2020). Numerous studies have demonstrated that the NGF/TrkA signaling pathway is essential for the plasticity and survival of forebrain cholinergic neurons in the hippocampus and cortex (Sánchez-Infantes et al., 2018), regions responsible for learning and memory. The upregulation of NGF/TrkA has been shown to mitigate radiation-induced neurogenesis deficits and cognitive impairments by activating PI3K/AKT signaling (Ji et al., 2020). In populations with cognitive impairments, including individuals with intellectual disabilities, serum NGF levels have been found to be significantly lower than those in healthy individuals. Consequently, NGF has been recognized as a potential serum biomarker for intellectual disability (Tuon et al., 2023; Malewska-Kasprzak et al., 2024). It has been reported that exogenous NGF supplementation can effectively prevent arsenic-induced neurotoxicity in PC12 cells by activating AKT-related pathways (Tan et al., 2019). However, whether arsenic affects NGF levels in humans and whether NGF downregulation contributes to arsenic-induced mitochondrial dynamics imbalance remain to be elucidated.

In this study, we investigated whether arsenic exposure leads to a decrease in NGF, thereby inducing mitochondrial dysregulation, neuronal damage, and cognitive impairment. Furthermore, using both a mouse model and HT-22 cells, we examined whether inactivation of the PI3K/AKT signaling pathway mediates these detrimental effects. Finally, through cell-based

experiments, we explored the mechanistic role of this pathway in arsenic-induced neurotoxicity. Our findings provide a theoretical foundation for understanding the mechanisms of arsenic-induced neurotoxicity and may inform future therapeutic strategies.

2 Materials and methods

2.1 Reagents

Sodium arsenite ($NaAsO_2$) was purchased from Sigma-Aldrich (Saint Louis, USA). Detailed information regarding other reagents is provided in Table S1.

2.2 Cell culture and animal experimental procedures

2.2.1 Cell culture and transfection

HT-22 cells (Procell, Wuhan, China) were seeded at a density of 2×10^5 cells per 25 mL culture flask and incubated for 12 h. A mixture was prepared containing 400 μL of NGF lentivirus (GenePharma, Shanghai, China) stock solution with a concentration of 1×10^9 TU/mL (transducing unit per mL) and 3600 μL of Dulbecco's modified Eagle's medium (DMEM) containing 10 g/L fetal bovine serum (FBS), to form a final concentration of 1×10^8 TU/mL. After thorough mixing, 3.6 mL of RPMI-1640 (GIBCO, Invitrogen, Carlsbad, USA) supplemented with 0.1 g/mL FBS and 5 μg/mL polyamine was added. Following incubation at 37 °C and 5% CO_2, the cell status was assessed. Successfully transfected cells were selected using 1 μg/mL puromycin (Solarbio, Beijing, China) for an additional 24 h. The experiments revealed that treatment with 2 μmol/L $NaAsO_2$ significantly induced apoptosis in HT-22 cells, while exposure to 4 μmol/L $NaAsO_2$ reduced the cell survival rate to below 50%. Therefore, we chose these two concentrations for our study.

2.2.2 Cell counting kit-8 assay

Cell viability was measured using a cell counting kit-8 (CCK-8) assay kit (Biosharp, Hefei, China). HT-22 cells were cultured at 3000 cells/well in a 96-well plate and incubated at 37 °C with 5% CO_2 for 24 h. Once cell adhesion was complete, cells were exposed to varying concentrations of arsenic for 24 h. Absorbance at 450 nm was measured using a microplate reader (Bio-Rad, California, USA) following the manufacturer's protocol.

2.2.3 Apoptosis assay

Apoptosis was detected using the Annexin V–fluorescein isothiocyanate (FITC) apoptosis detection kit (BD, New York, USA). Approximately 10 μL of propidium iodide (PI), 5 μL of membrane-associated Annexin V, and 500 μL of 1× binding buffer were added to each bottle of HT-22 cells (1×10^5 cells), which were then resuspended and incubated for 12 min. The fluorescence intensity of cells was analyzed using a flow cytometer (BD Accuri C6 Plus, USA). FlowJo v10 (BD, Ashland, USA) was used to calculate the number of cells in different states.

2.2.4 Western blotting

Total protein was extracted using radioimmunoprecipitation assay (RIPA) lysis buffer (Beyotime, Shanghai, China) containing protease inhibitors (Roche, Indianapolis, USA) and phosphatase inhibitors (Beyotime). After lysis, the supernatant was collected by centrifugation and the protein concentration was quantified using a bicinchoninic acid (BCA) assay kit (Beyotime). Electrophoresis (80 V constant voltage) and membrane transfer (200 mA constant current) were carried out for durations adjusted to the molecular weights of the proteins. Equal protein amounts were separated and blocked overnight. Membranes were incubated with primary and secondary antibodies, washed and developed using an enhanced chemiluminescence (ECL) solution, and then incubated with secondary antibodies and visualized using an ECL detection system (Biosharp, Hefei, China). Goat anti-rabbit or anti-mouse immunoglobulin G (IgG) was purchased from ZSGB-BIO (Beijing, China). Equal proportions of solutions A and B were mixed to prepare the ECL working solution. The polyvinylidene fluoride (PVDF) membrane (Roche, Indianapolis, USA) was soaked in a dark solution for 1 min and scanned for color development. Protein blot images were captured by the Tanon 5200 Multi-Chemiluminescence Imaging System (Tanon, China) and quantified with ImageJ 2.0 software (NIH, Bethesda, USA). The detailed information on the antibodies used is shown in Table S2.

2.2.5 Immunofluorescence staining

Cells were washed three times, fixed with 4% (0.04 g/mL) paraformaldehyde, and incubated overnight at 4 °C with primary antibodies. Afterwards, the cells were incubated with a secondary antibody for 1 h. The details and dilution concentrations of the antibodies are

listed in Table S2. The observation was performed using a Zeiss confocal laser scanning microscope (Carl Zeiss AG, Oberkochen, Germany). Zeiss Zen software was utilized to capture images.

2.2.6 Transmission electron microscopy

Glutaraldehyde was used to fix HT-22 cells, which were stored at room temperature away from light for 30 min and then transferred to 4 ℃. After staining, they were observed under a transmission electron microscope (H-7650, Hitachi, Japan).

2.2.7 Design of animal experiment

The animal experimental design is shown in Fig. 1a. Forty 4-week-old male C57BL/6N mice were purchased from Charles River Experimental Animal Technology Co., Ltd. (Beijing, China), as this age marks a critical period of maturation of the nervous system. After one week of adaptive feeding, the mice were randomly divided into three groups of 10 each. The control mice were given distilled water, while the mice in the $NaAsO_2$ group were given 25 or 50 mg/L $NaAsO_2$ for 12 weeks. The dosage of arsenic was selected based on our team's previous research (Lv et al., 2023). The experimental protocol was approved by the Ethics Committee of Harbin Medical University (Ethics Number: HRBMUECDC20210902).

2.2.8 Morris water maze test

The learning and memory abilities of mice were evaluated using the Morris water maze (MWM). The platform was located in the center of one quadrant of the test pool. The mice were randomly placed in one quadrant, and the time and trajectory to find the platform were recorded; if the time exceeded 60 s, the mice were guided to remain on the platform for 10 s. The mice were trained four times a day for a total of 4 d. On the 5th day, the platform was dismantled and the 60-s movement trajectory was observed. The trajectory was recorded by SMART 2.5 software (Panlab, Spain).

2.2.9 Determination of arsenic content in samples

Hydride generation-atomic fluorescence spectrometry (HG-AFS) with an AFS-933 instrument (Beijing Jitian Instruments Co., Ltd., Beijing, China) was employed to detect the total arsenic content in urine and brain tissues of mice. Specifically, a 5% (volume fraction) hydrochloric acid solution was used as the carrier solution and a 2% (0.02 g/mL) potassium borohydride solution as the reducing agent to measure the optical density (OD) of each sample and standard. Finally, the arsenic content of samples was obtained by the standard curve.

2.2.10 H&E, TUNEL, and Nissl staining

The paraffin-embedded tissues were sectioned to 4 μm thickness, and the slices were stained with hematoxylin and eosin (H&E; Biosharp, Hefei, China), terminal deoxynucleotidyl transferase dUTP nick-end labeling (TUNEL) detection reagents (Roche, Indianapolis, USA), and Nissl staining reagents (Solarbio, Beijing, China). The results were observed under a light microscope (Olympus BX53, Japan). The TUNEL and Nissl staining results were analyzed by Image-Pro Plus 6.0 software (Media Cybernetics, Silver Spring, USA).

2.2.11 Immunohistochemical staining

The immunohistochemical procedures were based on the methods used in our previous study (Ding et al., 2023). The detailed information on the antibodies used is shown in Table S2. Hippocampal tissues were observed under a microscope (Olympus BX53), and protein expression in the cells was quantified and analyzed using Image-Pro Plus 6.0 software.

2.3 Statistical analysis

The MWM escape latency data were analyzed using repeated-measures analysis of variance (ANOVA). The long axis (the longest diameter) and short axis (the longest diameter perpendicular to the long axis) of each mitochondrion in the transmission electron microscopy (TEM) field of view were measured using ImageJ software. At least three independent biological replicates were selected for each group of samples, with three TEM images taken for each replicate. The aspect ratio was calculated as the long axis length divided by the short axis length. Comparisons among multiple groups were analyzed using one-way ANOVA. $P<0.05$ was considered statistically significant.

3 Results

3.1 Effects of $NaAsO_2$ on brain-to-body ratio and cognitive performance in mice

To investigate the effects of arsenic exposure on body weight, brain arsenic accumulation, and cognitive

function, mice were subjected to 12-week $NaAsO_2$ treatment, and their neurotoxic effects were evaluated by brain-to-body ratio analysis and the MWM test. At the end of the 12-week exposure period, there were no significant differences in brain weight among the three groups of mice. Meanwhile, body weight increased over time in all three groups throughout the experimental period (Figs. S1a and S1b). At the end of the 12th week, the body weights of mice treated with 25 and 50 mg/L $NaAsO_2$ were significantly lower than those in the control group (P<0.05 and P<0.001; Fig. 1b). In contrast, the brain-to-body ratios of mice treated with 50 mg/L $NaAsO_2$ were significantly higher than those in the control group (P<0.001; Fig. 1c). Compared to the control group, the brain total arsenic levels of mice treated with 25 and 50 mg/L $NaAsO_2$ were significantly increased (P<0.001; Fig. 1d). Similarly, the urine total arsenic levels in these groups were significantly higher than those in the control group (P<0.05 and P<0.001; Fig. 1e).

In the MWM trials, the time required for mice to locate the hidden platform decreased with training progression (Fig. 1f). On the 5th day of the spatial probe test (SPT), mice treated with 25 and 50 mg/L $NaAsO_2$ exhibited a significantly lower frequency of platform crossings (P<0.01 and P<0.001; Fig. 1g) and reduced time spent in the target quadrant compared to the control mice (P<0.01 and P<0.001; Fig. 1h). In addition, the movement distances of mice in the 50 mg/L $NaAsO_2$ group within the target quadrant were significantly shorter than those of the control mice (P<0.05; Fig. 1i). As shown in Fig. 1j, the trajectories of the control mice are concentrated around the platform location, whereas those of $NaAsO_2$-treated mice are more dispersed. These results indicate that increasing the $NaAsO_2$ concentration leads to arsenic accumulation, weight loss, and memory impairment in mice.

3.2 Apoptosis of hippocampal neurons induced by $NaAsO_2$

To elucidate the effects of arsenic exposure on the structure and apoptosis of hippocampal neurons, we analyzed the pathological changes and apoptotic characteristics of mouse hippocampal tissues using H&E staining, Nissl staining, TUNEL apoptosis assay, and TEM. The H&E staining revealed that the cells in the cornu ammonis 1 (CA1) and CA3 regions of the hippocampi of control mice were tightly arranged with blue nuclei, whereas the cells of mice treated with 25 and 50 mg/L $NaAsO_2$ exhibited irregular arrangements, blurred shapes, and a reduced number of cells (Fig. 2a). Compared to the control mice, the Nissl-positive cell counts in the hippocampal CA3 region of mice treated with 25 and 50 mg/L $NaAsO_2$ and in the hippocampal dentate gyrus (DG) region of those treated with 50 mg/L $NaAsO_2$ were significantly reduced (P<0.05; Figs. 2b and 2c). Compared with that in the control mice, the apoptosis rate of hippocampal CA1 cells in the 50 mg/L $NaAsO_2$ group was significantly increased (P<0.01; Figs. 2d and 2e). The TEM results (Fig. 2f) showed that control mice exhibited intact nuclear membranes and chromatin aggregation. In contrast, mice treated with 25 mg/L $NaAsO_2$ displayed increased lipofuscin accumulation and mitochondrial swelling. More severe ultrastructural changes, including organelle depletion and nuclear membrane disruption, were observed in response to 50 mg/L $NaAsO_2$ treatment, indicating that $NaAsO_2$ causes apoptosis and ultrastructural damage in the hippocampal neurons of mice.

In addition, it was found that both 2 and 4 μmol/L $NaAsO_2$ significantly reduced HT-22 cell viability in the hippocampal neurons of mice (P<0.01 and P<0.001; Fig. 2g), with reductions of 25% and 60%, respectively. Meanwhile, the cleaved-caspase-3/caspase-3 ratio in the HT-22 cells of mice treated with 4 μmol/L $NaAsO_2$ was significantly elevated compared to the control group (P< 0.01; Figs. 2h and 2i). Moreover, both late-stage and total apoptosis rates of HT-22 cells exposed to 2 and 4 μmol/L $NaAsO_2$ were significantly higher than those in the control cells (P<0.01; Figs. 2j–2l). These results suggest that $NaAsO_2$ exposure significantly induces apoptosis in HT-22 cells.

3.3 Mitochondrial dynamics imbalance in hippocampal neurons induced by $NaAsO_2$

To reveal the effects of arsenic exposure on mitochondrial structure and dynamics, TEM observation and protein expression analysis were performed. As shown in Fig. 3a, control HT-22 cells contained more normal mitochondria with intact structures than HT-22 cells treated with 2 and 4 μmol/L $NaAsO_2$, in which the mitochondria were swollen and structurally abnormal. Further statistical analysis of the mitochondrial aspect ratio and morphology within the TEM field of view revealed that the mitochondrial aspect

ratio in the 4 μmol/L $NaAsO_2$ group was significantly decreased (P<0.05; Fig. 3b), while the proportion of swollen mitochondria among the total number of mitochondria in the 2 and 4 μmol/L $NaAsO_2$ groups was significantly increased (P<0.001 and P<0.0001; Fig. 3c).

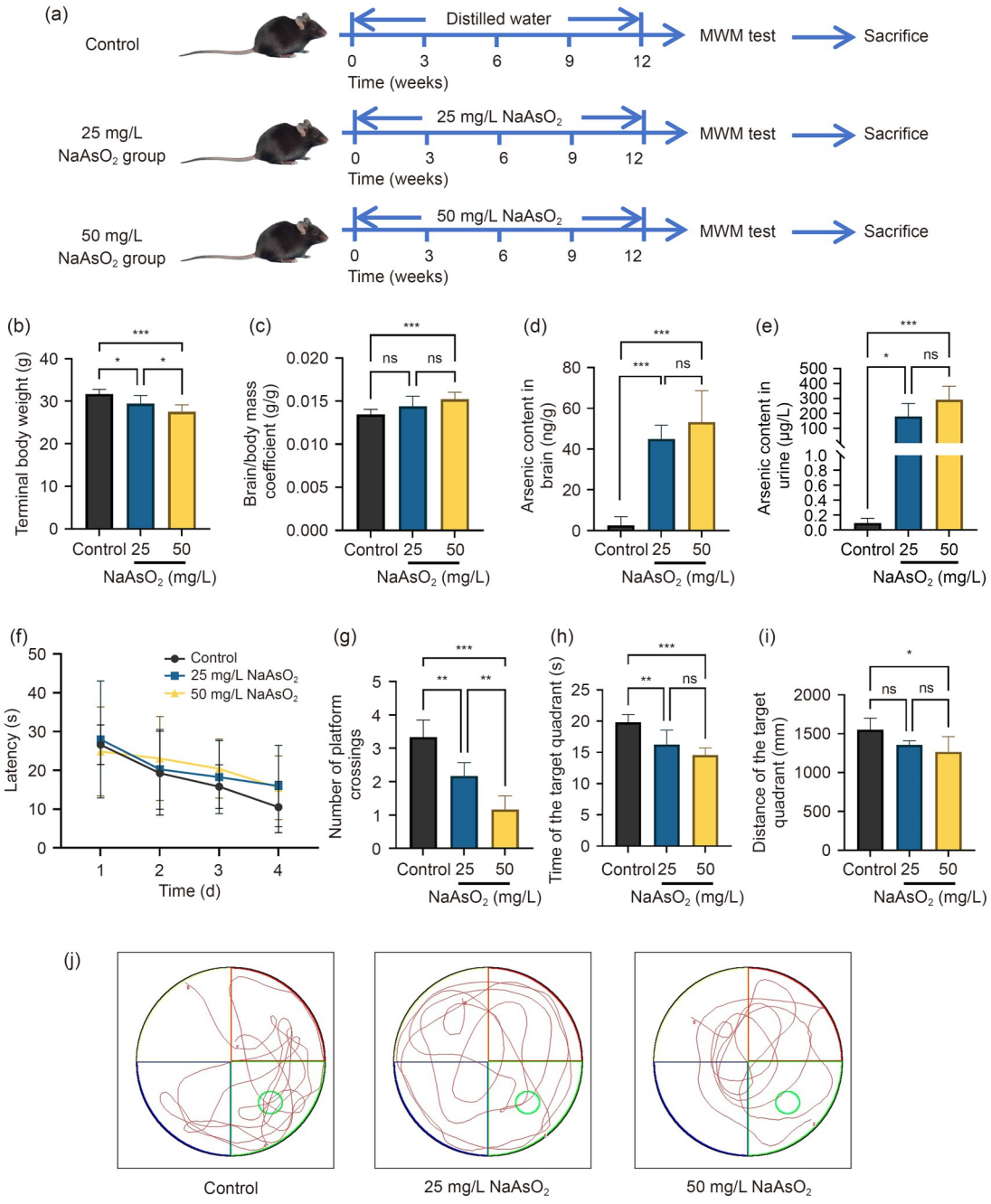

Fig. 1 Effects of sodium arsenite ($NaAsO_2$) on the brain-to-body ratio and cognitive performance in mice. (a) Schematic diagram of the animal experimental design. (b) Final body weight of each group of mice, n=10. (c) Changes in the brain-to-body ratio of each group of mice, n=10. (d) Total arsenic content in the brain tissue of each group of mice, n=10. (e) Total arsenic level in the urine of each group of mice, n=4. (f) Mean escape to platform latency was recorded during the first 4 d of the Morris water maze (MWM) navigation experience, n=10. (g) The number of times mice in each group crossed the platform, n=10. (h) The time mice in each group stayed in the target quadrant, n=10. (i) The distance mice in each group moved in the target quadrant, n=10. (j) Representative trajectories for the spatial probe test. The values are expressed as mean±standard deviation (SD). * P<0.05, ** P<0.01, and *** P<0.001; ns: no significance.

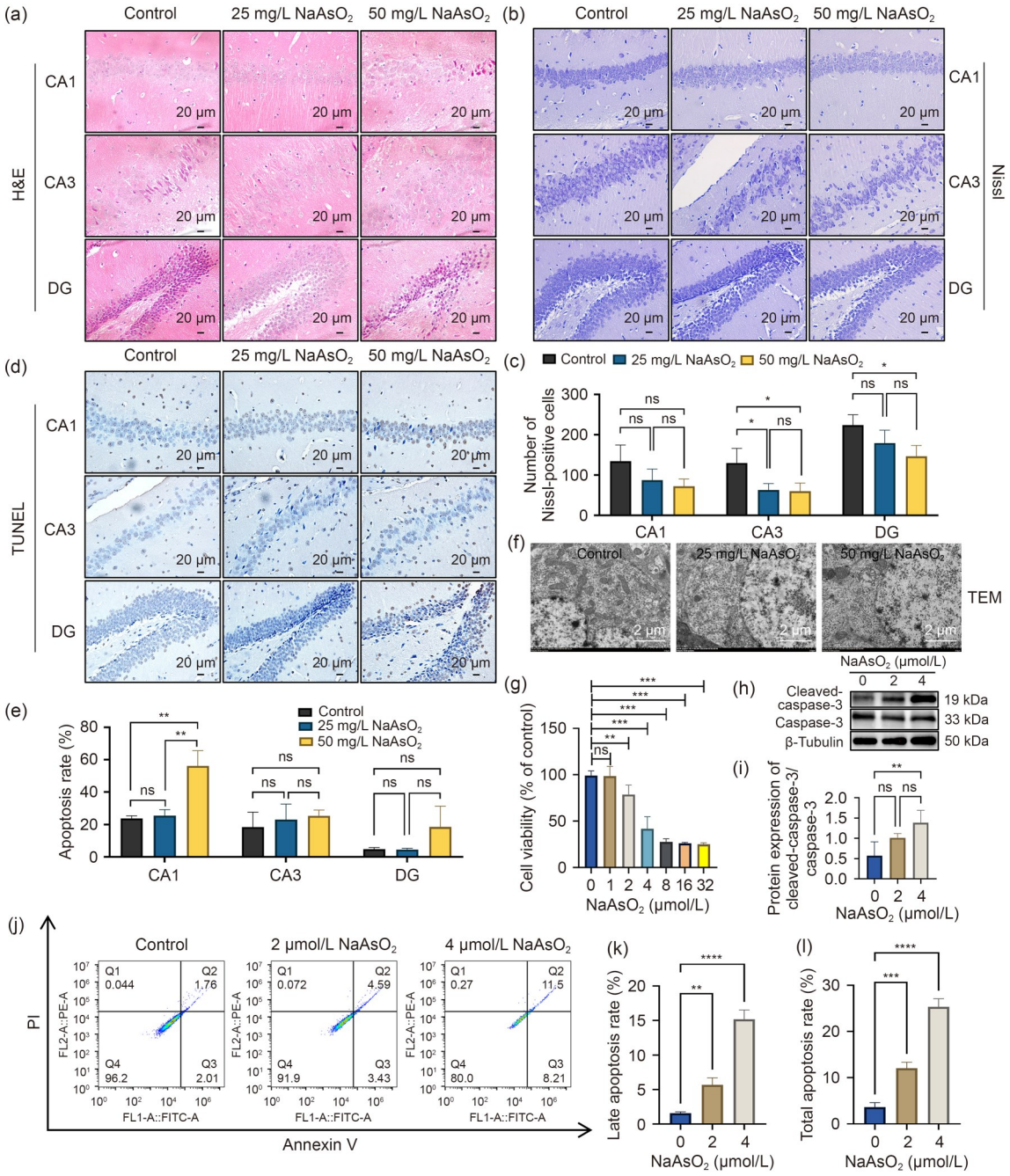

Fig. 2 Sodium arsenite ($NaAsO_2$)-induced structural abnormalities and apoptosis of hippocampal neurons. (a) Hematoxylin and eosin (H&E) staining of various regions in the hippocampus of mice, *n*=5. (b) Representative images of Nissl staining in various regions of the hippocampus. (c) Dark purple staining is considered a normal Nissl body structure, and the number of Nissl-positive cells represents the analysis results, *n*=3. (d) Representative images of terminal deoxynucleotidyl transferase dUTP nick-end labeling (TUNEL)-positive cells in various hippocampal regions, with yellowish brown-stained nuclei considered TUNEL-positive nuclei. (e) Apoptosis rates in various regions of the hippocampus, expressed as a percentage of TUNEL-positive cells to the total number of cells, *n*=3. (f) Transmission electron microscopy (TEM) was used to observe the ultrastructure of hippocampal neurons in mice. (g) Effect of $NaAsO_2$ on the viability of HT-22 cells, *n*=3. (h, i) Western blotting and quantitative analysis of the protein abundance of cleaved-caspase-3/caspase-3 ratio, *n*=3. (j) Representative images of flow cytometry with Annexin V/propidium iodide (PI) staining. (k) Changes in the late apoptosis rate in different groups, *n*=3. (l) Changes in the total apoptosis rate in different groups, *n*=3. The values are expressed as mean±standard deviation (SD). $^{*}P<0.05$, $^{**}P<0.01$, $^{***}P<0.001$, and $^{****}P<0.0001$; ns: no significance. CA: cornu ammonis; DG: dentate gyrus; FL: fluorescence channel; A: area; PE: phycoerythrin; FITC: fluorescein isothiocyanate.

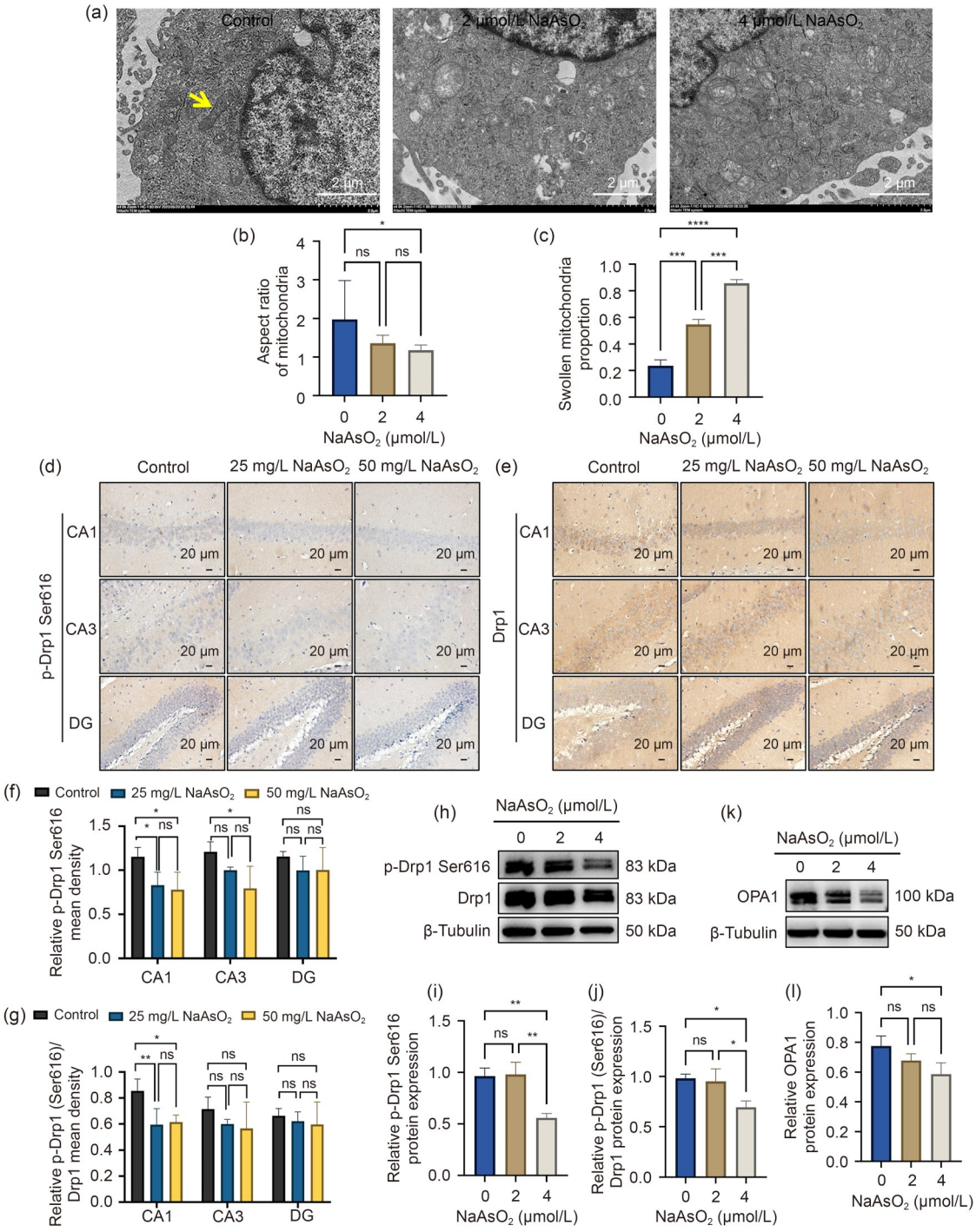

Fig. 3 Sodium arsenite ($NaAsO_2$)-induced mitochondrial dynamics imbalance in hippocampal neurons. (a) Transmission electron microscopy (TEM) was used to observe the morphology of mitochondria in HT-22 cells (yellow arrow: mitochondria with typical morphological characteristics). (b) Analysis of mitochondrial aspect ratio in TEM images for each group, *n*=3. (c) Ratio of the number of swollen mitochondria to the total number of mitochondria in TEM images for each group, *n*=3. (d, e) Immunohistochemistry was used to detect phosphorylated dynamin-related protein 1 (p-Drp1) Ser616 and Drp1 in various regions of the hippocampus. (f) Average optical density values of p-Drp1 Ser616 in the hippocampus, *n*=4. (g) The p-Drp1 (Ser616)/Drp1 ratio in the hippocampus, *n*=4. (h–l) Western blotting and quantitative analysis of the protein abundances of p-Drp1 Ser616, p-Drp1 (Ser616)/Drp1 ratio, and optic atrophy 1 (OPA1), *n*=3. The values are expressed as mean±standard deviation (SD). * *P*<0.05, ** *P*<0.01, *** *P*<0.001, and **** *P*<0.0001; ns: no significance. CA: cornu ammonis; DG: dentate gyrus.

Notably, p-Drp1 levels in hippocampal CA1 region were significantly reduced in mice treated with 25 and 50 mg/L $NaAsO_2$, while an obvious decline was only observed in the CA3 region at 50 mg/L dose ($P<0.05$; Figs. 3d and 3f). Additionally, Drp1 levels in the hippocampal CA1 region of 50 mg/L $NaAsO_2$-treated mice were significantly decreased compared to the control group ($P<0.05$; Figs. 3e and S1c). The p-Drp1/Drp1 ratio in the hippocampal CA1 region of $NaAsO_2$-treated mice was also significantly lower than that in the control group ($P<0.01$ and $P<0.05$; Fig. 3g). Similarly, in the HT-22 cells treated with 4 μmol/L $NaAsO_2$, both p-Drp1 levels and the p-Drp1/Drp1 ratio were significantly reduced compared to the control cells ($P<0.01$ and $P<0.05$; Figs. 3h–3j). Although Drp1 levels in HT-22 cells treated with 4 μmol/L $NaAsO_2$ showed a decreasing trend, the difference was not statistically significant (Fig. S1d). The expression of OPA1 in the 4 μmol/L $NaAsO_2$-treated HT-22 cells was significantly lower than that in the control cells ($P<0.05$; Figs. 3k and 3l).

3.4 $NaAsO_2$-mediated NGF downregulation and anti-apoptotic effects of NGF overexpression

To verify whether NGF downregulation is involved in arsenic-induced neuronal damage, we detected NGF expression in the hippocampus of mice and HT-22 cells after $NaAsO_2$ treatment and evaluated the neuroprotective effect of NGF through NGF overexpression experiments. As shown in Figs. 4a and 4b, NGF levels in the hippocampal CA1 and CA3 regions of $NaAsO_2$-treated mice were significantly lower than those in the control group ($P<0.01$ and $P<0.001$). A similar trend was observed in the $NaAsO_2$-treated HT-22 cells, as shown by immunofluorescence (Fig. 4c). Furthermore, the results of western blotting confirmed that the levels of NGF in HT-22 cells treated with 2 and 4 μmol/L $NaAsO_2$ were significantly lower than those in the control cells ($P<0.05$ and $P<0.01$; Figs. 4d and 4e).

Overexpression of NGF in HT-22 cells via transfection with an NGF lentiviral vector (LV) (Figs. 4f and 4g) substantially alleviated the $NaAsO_2$-induced increase in the cleaved-caspase-3/caspase-3 ratio ($P<0.01$; Figs. 4h and 4i) and decrease in cell viability ($P<0.05$; Fig. 4j). More importantly, the total and late-stage apoptosis rates of $NaAsO_2$-treated HT-22 cells overexpressing NGF were significantly reduced compared to those of $NaAsO_2$-treated HT-22 cells ($P<0.001$ and $P<0.0001$; Figs. 4k–4m). These results indicate that NGF overexpression mitigates the arsenic-induced apoptosis of HT-22 cells.

3.5 Amelioration of $NaAsO_2$-induced mitochondrial dynamics imbalance via NGF overexpression

To verify whether NGF exerts neuroprotective effects by regulating mitochondrial dynamics, NGF was overexpressed in $NaAsO_2$-treated HT-22 cells, and we further observed the changes in mitochondrial morphology, dynamics-related proteins, and apoptosis. As shown in Fig. 5a, NGF overexpression in HT-22 cells significantly counteracted $NaAsO_2$-induced mitochondrial swelling and restored more mitochondria with normal morphological characteristics. Further analysis showed that NGF overexpression significantly reversed the decrease in the mitochondrial aspect ratio and the increase in the proportion of swollen mitochondria among the total number of mitochondria in the $NaAsO_2$ group ($P<0.05$ and $P<0.01$; Figs. 5b and 5c). Additionally, NGF overexpression significantly reversed $NaAsO_2$-induced reductions in p-Drp1 levels, p-Drp1/Drp1 ratio, and OPA1 levels ($P<0.05$; Figs. 5d–5h), while the changes in Drp1 levels were not statistically significant (Fig. S1e). Immunofluorescence analysis further corroborated these findings, showing that NGF overexpression significantly restored p-Drp1 and OPA1 levels (Figs. 5i and 5j), whereas Drp1 levels remained unchanged (Fig. S1f). These results suggest that NGF overexpression mitigates the $NaAsO_2$-induced imbalance of mitochondrial dynamics.

3.6 Attenuation of arsenic-induced effects on PI3K/AKT signaling pathways by NGF

To clarify whether NGF-mediated neuroprotection depends on the PI3K/AKT signaling pathway, we detected the phosphorylation levels of PI3K and AKT and the expression of the downstream molecule adenosine triphosphate (ATP)-dependent metalloprotease (YME1L1) in the hippocampus of mice and HT-22 cells after arsenic exposure, and analyzed the regulatory effect of NGF on this pathway. The YME1L1 levels in the hippocampus of mice exposed to 50 mg/L $NaAsO_2$ were significantly lower than those in the control group ($P<0.001$; Figs. 6a and 6b), and 4 μmol/L $NaAsO_2$ significantly reduced YME1L1 levels in HT-22 cells compared to the control group ($P<0.01$; Figs. 6c

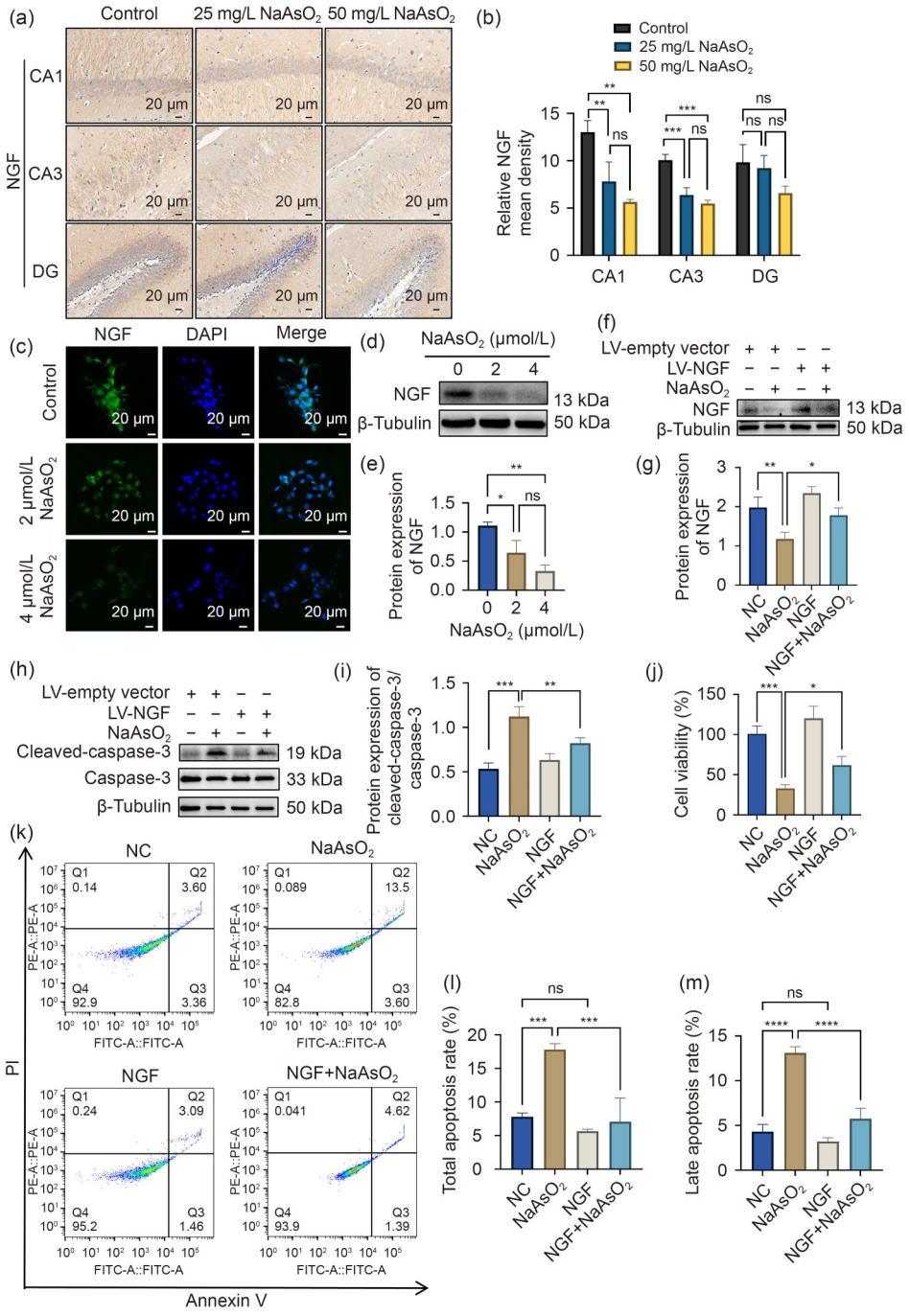

Fig. 4 Effects of overexpression of nerve growth factor (NGF) on sodium arsenite ($NaAsO_2$)-induced apoptosis. (a) Immunohistochemistry was used to detect NGF in various regions of the hippocampus. (b) Average optical density values of NGF in the hippocampus, *n*=4. (c) NGF fluorescence intensity in HT-22 cells treated with 2 and 4 μmol/L $NaAsO_2$ was observed using confocal microscopy, *n*=3. (d, e) Western blotting and quantitative analysis of NGF protein abundance in HT-22 cells after $NaAsO_2$ exposure, *n*=3. (f, g) Western blotting and quantitative analysis of NGF protein abundance in HT-22 cells after arsenic treatment and/or lentiviral transfection with NGF overexpression vector, *n*=3. (h, i) Western blotting and quantitative analysis of cleaved-caspase-3 expression, *n*=3. (j) Effect of $NaAsO_2$ on the viability of HT-22 cells after overexpression of NGF, *n*=3. (k) Representative images of flow cytometry with Annexin V/propidium iodide (PI) staining. (l, m) Changes of total and late apoptosis rates in different groups, *n*=3. The values are expressed as mean±standard deviation (SD). * *P*<0.05, ** *P*<0.01, *** *P*<0.001, and **** *P*<0.0001; ns: no significance. CA: cornu ammonis; DG: dentate gyrus; DAPI: 4',6-diamidino-2-phenylindole; LV: lentiviral vector; NC: normal control; PE: phycoerythrin; FITC: fluorescein isothiocyanate; A: area.

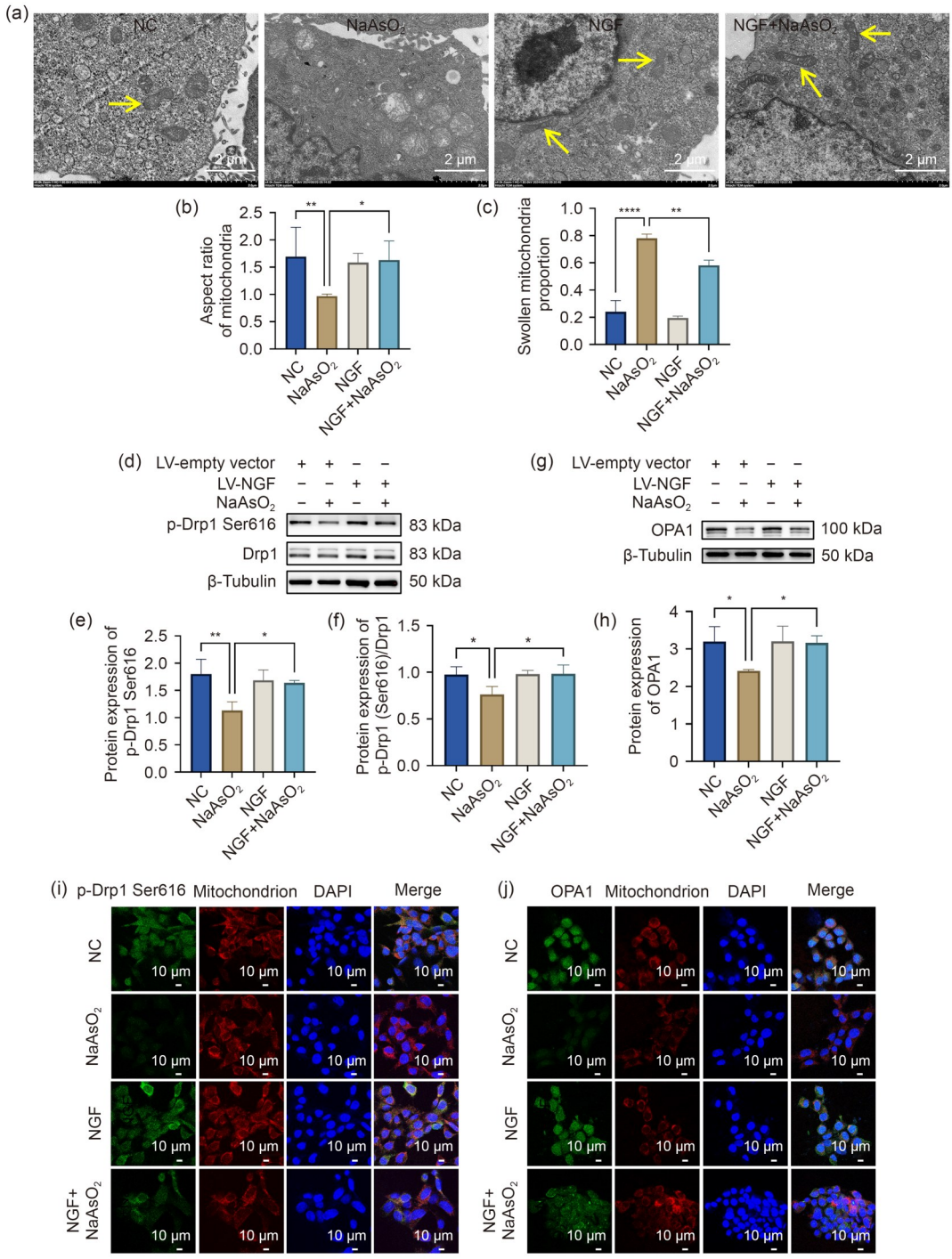

Fig. 5 Effects of overexpression of nerve growth factor (NGF) on mitochondrial dynamics imbalance caused by sodium arsenite ($NaAsO_2$). (a) Transmission electron microscopy (TEM) was used to observe the morphology of mitochondria in HT-22 cells (yellow arrow: mitochondria with typical morphological characteristics). (b) Analysis of the mitochondrial aspect ratio in TEM images for each group, *n*=3. (c) Ratio of the number of swollen mitochondria to the total number of mitochondria in TEM images for each group, *n*=3. (d–f) Western blotting and quantitative analysis of the protein abundance of phosphorylated dynamin-related protein 1 (p-Drp1) Ser616 and p-Drp1 (Ser616)/Drp1 ratio, *n*=3. (g, h) Western blotting and quantitative analysis of the protein abundance of optic atrophy 1 (OPA1), *n*=3. (i, j) The p-Drp1 Ser616 and OPA1 fluorescence intensities in HT-22 cells were observed using confocal microscopy, *n*=3. The values are expressed as mean±standard deviation (SD). * *P*<0.05, ** *P*<0.01, and **** *P*<0.0001. NC: normal control; LV: lentiviral vector; DAPI: 4',6-diamidino-2-phenylindole.

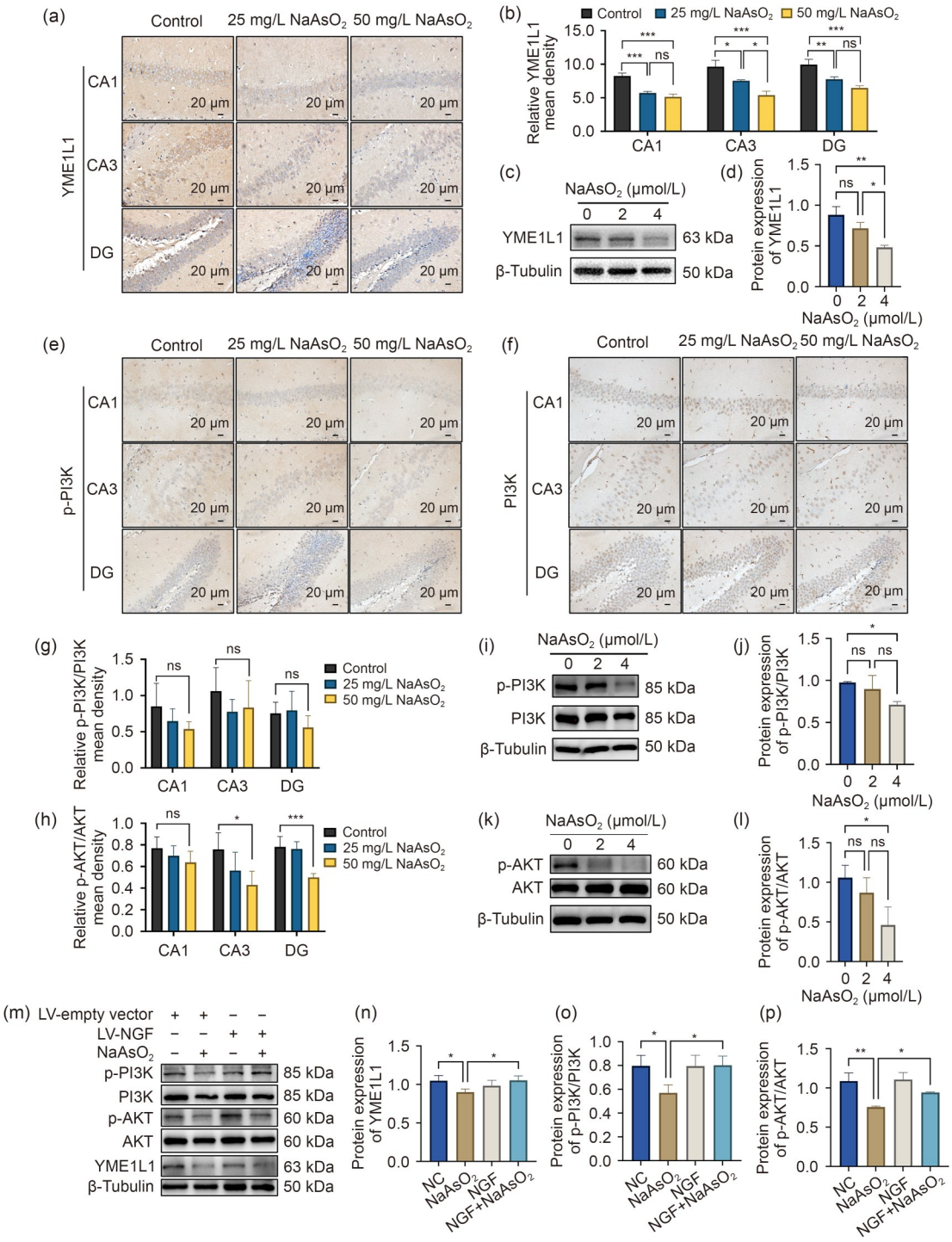

Fig. 6 Attenuation of arsenic-induced effects on phosphatidylinositol 3-kinase/protein kinase B (PI3K/AKT)-related signaling pathways by nerve growth factor (NGF). Immunohistochemistry was used to detect adenosine triphosphate (ATP)-dependent metalloprotease YME1L1 (a), phosphorylation of PI3K (p-PI3K) (e), and PI3K (f) in various regions of the hippocampus. Average optical density values of YME1L1 (b), p-PI3K/PI3K (g), and phosphorylation of AKT (p-AKT)/AKT (h) in the hippocampus, n=3. YME1L1 (c, d), p-PI3K/PI3K (i, j), and p-AKT/AKT (k, l) proteins in HT-22 cells treated with sodium arsenite ($NaAsO_2$) were detected by western blotting, n=3. (m–p) Immunoblotting was used to detect the protein contents of YME1L1, p-PI3K/PI3K, and p-AKT/AKT in HT-22 cells overexpressing NGF, n=3. The values are expressed as mean± standard deviation (SD). * P<0.05, ** P<0.01, and *** P<0.001; ns: no significance. CA: cornu ammonis; DG: dentate gyrus; NC: normal control; LV: lentiviral vector.

and 6d). As shown in Figs. S2a, S2b, and 6h, the p-AKT/AKT ratio in CA3 and DG regions of mouse hippocampi in the 50 mg/L $NaAsO_2$ group was significantly lower than that in the control group (P<0.05 and P<0.001). Although the p-PI3K/PI3K ratio was also reduced, the difference was not statistically significant (Figs. 6e–6g). The western blotting results revealed that the p-PI3K/PI3K and p-AKT/AKT ratios in HT-22 cells treated with 4 μmol/L $NaAsO_2$ were significantly lower than those in the control group (P<0.05; Figs. 6i–6l).

NGF overexpression reversed the reduction in the YME1L1 level, p-PI3K/PI3K ratio, and p-AKT/AKT ratio caused by 4 μmol/L $NaAsO_2$ (P<0.05; Figs. 6m–6p). These results indicate that NGF attenuates arsenic-induced disruptions in the PI3K/AKT-related signaling pathways.

3.7 Suppression of protective effects of NGF against $NaAsO_2$-induced mitochondrial dynamics imbalance by PI3K/AKT inhibition

To verify the necessity of the PI3K/AKT pathway in NGF-regulated mitochondrial dynamics, we inhibited this pathway using LY294002 and subsequently analyzed the signaling-dependent mechanism of NGF's protective effect by detecting the expression of mitochondria-related proteins and the apoptosis rate. As shown in Figs. 7a–7g, treatment with 20 μmol/L LY294002 significantly attenuated the protective effect of NGF overexpression against apoptosis in HT-22 cells and reduced the impact of arsenic exposure on the PI3K/AKT signaling pathway. Specifically, compared with the LV-NGF+$NaAsO_2$ group, the LV-NGF+$NaAsO_2$+LY294002 group exhibited a significant increase in cleaved-caspase-3/caspase-3 in HT-22 cells (P<0.05; Figs. 7f and 7g), while the p-PI3K/PI3K ratio, p-AKT/AKT ratio, and YME1L1 levels were significantly decreased (P<0.001, P<0.05, and P<0.05; Figs. 7a–7e).

Compared with the LV-NGF+$NaAsO_2$ group, LY294002 significantly weakened the protective effect of NGF overexpression against the decrease in the expression of p-Drp1, Drp1, and OPA1 and the p-Drp1/Drp1 ratio in HT-22 cells caused by arsenic exposure (P<0.001, P<0.05, P<0.05, and P<0.05; Figs. 7h–7l and S2c). Flow cytometry analysis demonstrated that, compared to HT-22 cells in the LV-NGF+$NaAsO_2$ group, those in the LV-NGF+$NaAsO_2$+LY294002 group had significantly increased total and late apoptosis rates (P<0.01 and P<0.001; Figs. 7m–7o). These findings indicate that LY294002 significantly reduces the inhibitory effects of NGF overexpression on arsenic-induced apoptosis in HT-22 cells.

4 Discussion

Studies have established that serum NGF is positively correlated with cognitive ability scores and NGF supplementation can improve cognitive function in patients (Olson, 1993; He et al., 2024). This has sparked our interest in exploring the role of NGF reduction in arsenic-induced cognitive impairment. Four-week-old mice correspond to human adolescence, during which the nervous system remains in a developmental stage (Kang et al., 2024). Arsenic exhibits more significant toxicity during this period, particularly affecting growth and development and metabolic homeostasis, and poses long-term health risks (Tolins et al., 2014). Our previous study (Lv et al., 2023) found that 25 and 50 mg/L $NaAsO_2$ could induce neural damage in 4-week-old mice. Therefore, in this study, we established a model of 4-week-old male mice treated with 25 and 50 mg/L $NaAsO_2$.

In our animal experiments, $NaAsO_2$ significantly inhibited the expression of NGF, accompanied by impaired learning and memory abilities, reduced hippocampal neurons, and increased apoptosis rates in mice. These findings indicate that our animal model was successfully established. Notably, although there was no significant difference in the brain arsenic and urine arsenic levels between the 25 and 50 mg/L groups, both brain arsenic (R=0.82, P<0.05) and urine arsenic (R=0.89, P<0.05) levels showed a significant positive correlation with the arsenic exposure dose. Indeed, the 50 mg/L group exhibited more pronounced effects on certain outcomes, such as body weight reduction, MWM performance, loss of Nissl-stained positive cells, and CA1 apoptosis. It has been reported that CA1 neurons are more susceptible to arsenic due to their higher energy demand (Wang and Michaelis, 2010), which may explain why the apoptosis rate in the CA1 region was significantly higher than that in the control group. Following treatment with 50 mg/L $NaAsO_2$, the numbers of Nissl-positive cells in the hippocampal CA3 and DG regions were significantly lower than those in the control group, with no corresponding increase in

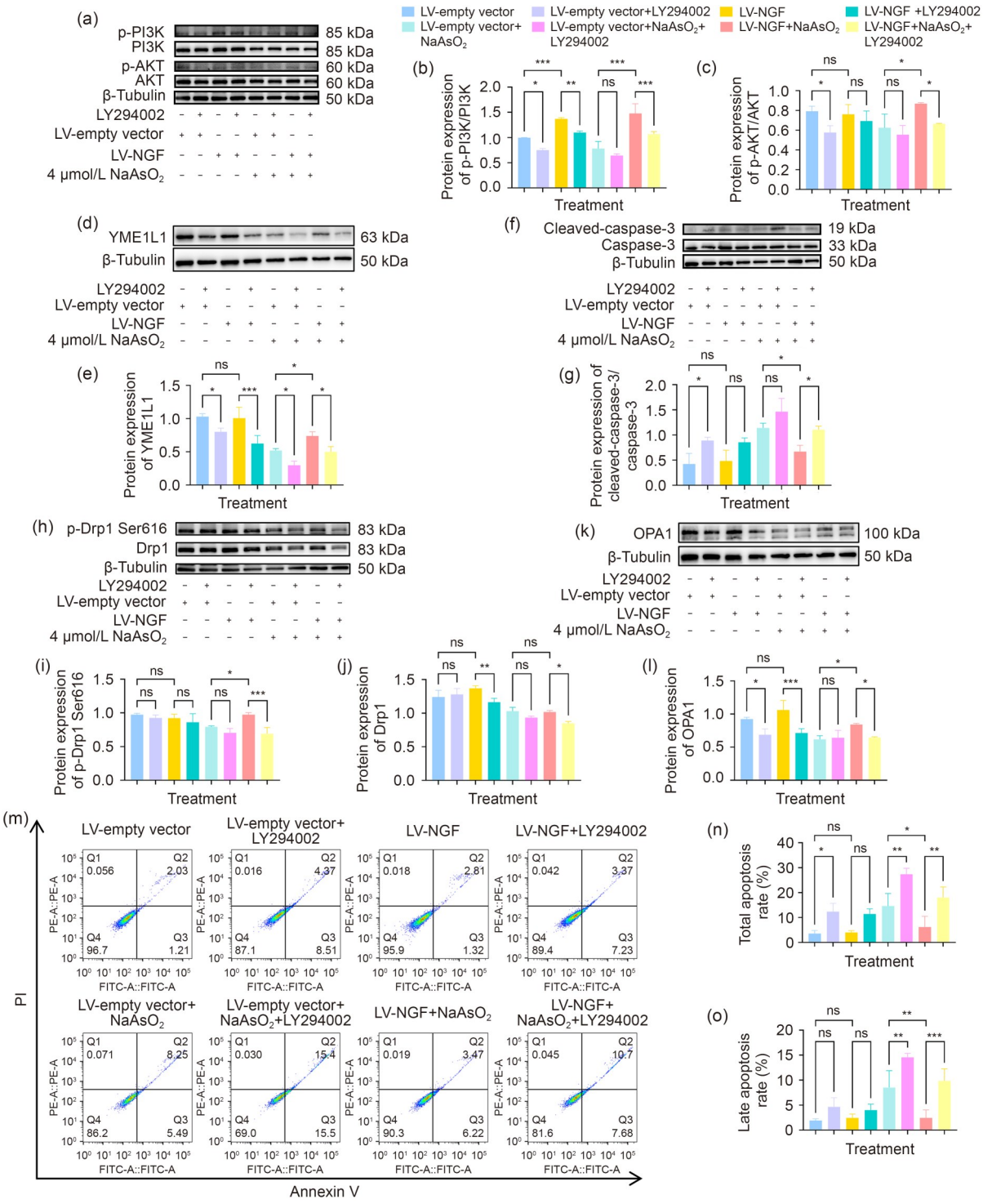

Fig. 7 Suppression of protective effects of NGF against $NaAsO_2$-induced mitochondrial dynamics imbalance by PI3K/AKT inhibition. Phosphorylation of PI3K (p-PI3K)/PI3K and phosphorylation of AKT (p-AKT)/AKT (a–c), ATP-dependent metalloprotease YME1L1 (d, e), cleaved-caspase-3/caspase-3 (f, g), phosphorylated dynamin-related protein 1 (p-Drp1) Ser616 and Drp1 (h–j), and optic atrophy 1 (OPA1) (k, l) proteins in HT-22 cells treated with LY294002 were detected by western blotting, *n*=3. (m) Representative images of flow cytometry with Annexin V/propidium iodide (PI) staining. (n, o) Changes in the total and late apoptosis rates in different groups, *n*=3. The values are expressed as mean±standard deviation (SD). * *P*<0.05, ** *P*<0.01, and * *P*<0.001; ns: no significance. LV: lentiviral vector; PE: phycoerythrin; FITC: fluorescein isothiocyanate; A: area.**

apoptosis rates; in contrast, elevated apoptosis was exclusively observed in the CA1 region. TUNEL positivity specifically reflects apoptotic events, while Nissl staining primarily reveals large-scale cell loss resulting from apoptosis, necrosis, or non-apoptotic cell death. Therefore, these findings suggest that non-apoptotic cell death pathways may more prominently mediate arsenic-induced loss of Nissl-positive cells in the hippocampal CA3 and DG regions. Notably, in vitro studies further confirmed that $NaAsO_2$ induces apoptosis and ultrastructural damage in HT-22 cells. NGF is widely recognized as a key regulator of neural function, and its downregulation may contribute to neuronal damage and cognitive impairment. Importantly, NGF treatment has been shown to improve cognitive function (Lu CL et al., 2023). Thus, we hypothesized that reduced NGF levels are a key factor in arsenic-induced neurotoxicity. It is well-known that the regulatory mechanisms of NGF expression involve multiple factors, such as oxidative stress, epigenetic modifications, and non-coding RNAs (Heberlein et al., 2013; Tsai et al., 2014); therefore, the specific mechanisms by which arsenic affects NGF levels remain to be further investigated.

Studies have highlighted that NGF enhances mitochondrial dynamics by upregulating mitochondrial fusion- and fission-related proteins, thereby promoting normal neuronal differentiation (Martorana et al., 2018; Goglia et al., 2024). Drp1 is a key regulator of mitochondrial fission, and p-Drp1 modulates the localization and aggregation of Drp1 in mitochondria, affecting the process of mitochondrial fission (Schmitt et al., 2018; Gao et al., 2022). OPA1, located in the inner mitochondrial membrane, plays a crucial role in maintaining the structure of mitochondrial cristae and genome stability (Frezza et al., 2006). The interaction and balance of these fusion- and fission-related proteins are essential for mitochondrial integrity and function. Under pathological conditions, dysregulation of p-Drp1, Drp1, and OPA1 may lead to mitochondrial dysfunction, resulting in cell death and tissue damage (Qin and Xi, 2022). Martorana et al. (2018) found that NGF-induced neuronal differentiation is accompanied by increased mitochondrial remodeling, as evidenced by the upregulation of p-Drp1 and OPA1. Our results indicate that $NaAsO_2$ significantly disrupts mitochondrial fusion and fission, leading to mitochondrial swelling and cristae dissipation. We hypothesized that arsenic-induced mitochondrial alterations may be linked to the dysregulation of mitochondrial dynamics-related proteins, including p-Drp1, Drp1, and OPA1. Consistent with this hypothesis, the levels of mitochondrial fission-related proteins p-Drp1 and Drp1 and fusion protein OPA1 were significantly reduced in arsenic-treated mice and HT-22 cells. Previous studies have shown that the protection of damaged neurons by stimulating NGF release is associated with the activation of the PI3K/AKT cell survival signaling pathway (Sang et al., 2018). Combined with the findings of this study, the protective effect of NGF on neurons may be related to its alleviation of mitochondrial dynamics imbalance via the PI3K/AKT pathway. Therefore, we speculate that arsenic can further inhibit p-Drp1 and OPA1 by reducing NGF, thereby damaging mitochondrial dynamics and ultimately leading to neurotoxicity.

The PI3K/AKT pathway has been shown to regulate the phosphorylation level of Drp1 and the level of OPA1 to maintain mitochondrial homeostasis and normal function (Kim et al., 2016; Wang et al., 2023). In the present study, $NaAsO_2$ significantly reduced the levels of p-PI3K/PI3K and p-AKT/AKT in the hippocampal tissues of mice and HT-22 cells, indicating that $NaAsO_2$ can inactivate the PI3K/AKT signaling pathway, consistent with previous reports (Goussetis and Platanias, 2010). Further research has shown that NGF overexpression alleviates the inhibitory effect of arsenic on AKT activation. In addition, arsenic exposure significantly reduced the expression of YME1L1, a lytic enzyme involved in OPA1 activation, whose deficiency leads to cell proliferation defects and mitochondrial fusion disorders (Hartmann et al., 2016). Our research suggests that arsenic suppresses mitochondrial fusion by inhibiting PI3K/AKT phosphorylation via NGF reduction, which may be related to the reduction in YME1L1. Previous studies have shown that NGF activates PI3K/AKT cell survival signaling to promote neuronal survival and enhance mitochondrial length and density (Sang et al., 2018; Armijo-Weingart et al., 2019). In our study, LY294002, an inhibitor of the PI3K/AKT signaling pathway, significantly antagonized the protective effects of NGF on the expression of p-Drp1, Drp1, and OPA1 and cell viability. These findings suggest that arsenic-induced NGF reduction inhibits mitochondrial dynamics via the PI3K/AKT pathway, ultimately leading to cognitive impairment. It is worth noting that NGF exerts its effects by binding to its receptor TrkA and

may also influence neuronal survival through alternative pathways, such as the phospholipase C gamma (PLC-γ) (Huang and Reichardt, 2003; Calvo-Enrique et al., 2023). Future genetic intervention studies targeting TrkA and PLC-γ are necessary to further elucidate these mechanisms.

5 Conclusions

Arsenic-induced cognitive impairment and neuronal damage were found to be associated with NGF downregulation and mitochondrial dynamics imbalance. Furthermore, NGF supplementation mitigated these effects, with the PI3K/AKT pathway playing a crucial role in the neuroprotective response to arsenic exposure. These findings provide novel insights into the mechanisms underlying arsenic-induced neurotoxicity and suggest that NGF-mediated mitochondrial regulation may serve as a potential therapeutic target for arsenic-related neurological disorders.

Data availability statement

The datasets used and analyzed during the current study are available from the corresponding authors upon reasonable request.

Acknowledgments

This work was supported by the Harbin Medical University (HMU) Marshal Initiative Funding (No. HMUMIF-21014), China.

Author contributions

Xinbo MA: methodology, writing – original draft, and software. Liu YANG: writing – review and editing. Xinhua SHAO, Jia CUI, Ziqiao GUAN, Man LYU, Shuaifei YANG, Na FANG, and Yang LIU: methodology. Yanhui GAO: conceptualization. Xiaona LIU: conceptualization, writing – review and editing, and funding acquisition. Yanmei YANG: conceptualization, writing – review and editing, data curation, and funding acquisition. All authors have read and approved the final manuscript, and therefore, have full access to all the data in the study and take responsibility for the integrity and security of the data.

Compliance with ethics guidelines

Xinbo MA, Liu YANG, Xinhua SHAO, Jia CUI, Ziqiao GUAN, Man LYU, Shuaifei YANG, Na FANG, Yang LIU, Yanhui GAO, Xiaona LIU, and Yanmei YANG declare that they have no conflicts of interest.

Animal experimentation was approved by the Ethics Committee of the Center for Endemic Disease Control, Chinese Center for Disease Control and Prevention, Harbin Medical University (No. HRBMUECDC20210902). The approval certificate can be provided on request.

Declaration on the use of generative AI tools

No generative AI tools were used in the preparation of this manuscript.

References

Armijo-Weingart L, Ketschek A, Sainath R, et al., 2019. Neurotrophins induce fission of mitochondria along embryonic sensory axons. *eLife*, 8:e49494. https://doi.org/10.7554/eLife.49494

Baruch-Eliyahu N, Rud V, Braiman A, et al., 2019. Telomerase increasing compound protects hippocampal neurons from amyloid beta toxicity by enhancing the expression of neurotrophins and plasticity related genes. *Sci Rep*, 9:18118. https://doi.org/10.1038/s41598-019-54741-7

Bertholet AM, Delerue T, Millet AM, et al., 2016. Mitochondrial fusion/fission dynamics in neurodegeneration and neuronal plasticity. *Neurobiol Dis*, 90:3-19. https://doi.org/10.1016/j.nbd.2015.10.011

Bozack AK, Hall MN, Liu XH, et al., 2019. Folic acid supplementation enhances arsenic methylation: results from a folic acid and creatine supplementation randomized controlled trial in Bangladesh. *Am J Clin Nutr*, 109(2):380-391. https://doi.org/10.1093/ajcn/nqy148

Calvo-Enrique L, Lisa S, Vicente-García C, et al., 2023. Enhanced TrkA signaling impairs basal forebrain-dependent behavior. *Front Mol Neurosci*, 16:1266983. https://doi.org/10.3389/fnmol.2023.1266983

Chen W, Zhao HK, Li YS, 2023. Mitochondrial dynamics in health and disease: mechanisms and potential targets. *Signal Transduct Target Ther*, 8:333. https://doi.org/10.1038/s41392-023-01547-9

Cho HK, Kim W, Lee KY, et al., 2020. Beta-nerve growth factor gene therapy alleviates pyridoxine-induced neuropathic damage by increasing doublecortin and tyrosine kinase A in the dorsal root ganglion. *Neural Regen Res*, 15(1):162-168. https://doi.org/10.4103/1673-5374.264472

Cronican AA, Fitz NF, Carter A, et al., 2013. Genome-wide alteration of histone H3K9 acetylation pattern in mouse offspring prenatally exposed to arsenic. *PLoS One*, 8(2):e53478. https://doi.org/10.1371/journal.pone.0053478

Ding B, Ma XB, Liu Y, et al., 2023. Arsenic-induced, mitochondria-mediated apoptosis is associated with decreased peroxisome proliferator-activated receptor γ coactivator α in rat brains. *Toxics*, 11(7):576. https://doi.org/10.3390/toxics11070576

Fei DX, Zhao HJ, Wang Y, et al., 2019. The disturbance of autophagy and apoptosis in the gizzard caused by copper and/or arsenic are related to mitochondrial kinetics. *Chemosphere*, 231:1-9. https://doi.org/10.1016/j.chemosphere.2019.05.101

Frezza C, Cipolat S, Martins de Brito O, et al., 2006. OPA1 controls apoptotic cristae remodeling independently from

mitochondrial fusion. *Cell*, 126(1):177-189. https://doi.org/10.1016/j.cell.2006.06.025

Gao QT, Tian RY, Han HL, et al., 2022. PINK1-mediated Drp1^{S616} phosphorylation modulates synaptic development and plasticity via promoting mitochondrial fission. *Signal Transduct Target Ther*, 7:103. https://doi.org/10.1038/s41392-022-00933-z

Goglia I, Węglarz-Tomczak E, Gioia C, et al., 2024. Fusion-fission-mitophagy cycling and metabolic reprogramming coordinate nerve growth factor (NGF)-dependent neuronal differentiation. *FEBS J*, 291(13):2811-2835. https://doi.org/10.1111/febs.17083

Goussetis DJ, Platanias LC, 2010. Arsenic trioxide and the phosphoinositide 3-kinase/Akt pathway in chronic lymphocytic leukemia. *Clin Cancer Res*, 16(17):4311-4312. https://doi.org/10.1158/1078-0432.CCR-10-1496

Hartmann B, Wai T, Hu H, et al., 2016. Homozygous *YME1L1* mutation causes mitochondriopathy with optic atrophy and mitochondrial network fragmentation. *eLife*, 5:e16078. https://doi.org/10.7554/eLife.16078

He MY, Liu Z, Lian TH, et al., 2024. Role of nerve growth factor on cognitive impairment in patients with Alzheimer's disease carrying apolipoprotein E ε4. *CNS Neurosci Ther*, 30(6):e14560. https://doi.org/10.1111/cns.14560

Heberlein A, Muschler M, Frieling H, et al., 2013. Epigenetic down regulation of nerve growth factor during alcohol withdrawal. *Addict Biol*, 18(3):508-510. https://doi.org/10.1111/j.1369-1600.2010.00307.x

Hong YS, Song KH, Chung JY, 2014. Health effects of chronic arsenic exposure. *J Prev Med Public Health*, 47(5):245-252. https://doi.org/10.3961/jpmph.14.035

Huang EJ, Reichardt LF, 2003. Trk receptors: roles in neuronal signal transduction. *Annu Rev Biochem*, 72:609-642. https://doi.org/10.1146/annurev.biochem.72.121801.161629

Ishihara N, Nomura M, Jofuku A, et al., 2009. Mitochondrial fission factor Drp1 is essential for embryonic development and synapse formation in mice. *Nat Cell Biol*, 11:958-966. https://doi.org/10.1038/ncb1907

Jeong S, Ahn C, Kwon JS, et al., 2023. Effects of sodium arsenite on the myocardial differentiation in mouse embryonic bodies. *Toxics*, 11(2):142. https://doi.org/10.3390/toxics11020142

Ji SJ, Wu HH, Ding X, et al., 2020. Increased hippocampal TrkA expression ameliorates cranial radiation-induced neurogenesis impairment and cognitive deficit via PI3K/AKT signaling. *Oncol Rep*, 44(6):2527-2536. https://doi.org/10.3892/or.2020.7782

Kang JY, Lee JS, Wang JH, et al., 2024. Sleep deprivation in adolescent mice impairs long-term memory till early adulthood via suppression of hippocampal astrocytes. *Sleep*, 47(10):zsae143. https://doi.org/10.1093/sleep/zsae143

Kim DI, Lee KH, Gabr AA, et al., 2016. Aβ-induced Drp1 phosphorylation through Akt activation promotes excessive mitochondrial fission leading to neuronal apoptosis. *Biochim Biophys Acta-Mol Cell Res*, 1863(11):2820-2834. https://doi.org/10.1016/j.bbamcr.2016.09.003

Liu JT, Bain LJ, 2018. Arsenic induces members of the mmu-miR-466-669 cluster which reduces NeuroD1 expression. *Toxicol Sci*, 162(1):64-78. https://doi.org/10.1093/toxsci/kfx241

Liu YC, Zhao HJ, Wang Y, et al., 2020. Arsenic (III) and/or copper (II) induces oxidative stress in chicken brain and subsequent effects on mitochondrial homeostasis and autophagy. *J Inorg Biochem*, 211:111201. https://doi.org/10.1016/j.jinorgbio.2020.111201

Lu CL, Li S, Kang L, et al., 2023. Aripiprazole combined with nerve growth factor improves cognitive function in mice with schizophrenia model. *Neurosci Lett*, 812:137410. https://doi.org/10.1016/j.neulet.2023.137410

Lu HM, Yin K, Su H, et al., 2023. Polystyrene microplastics induce autophagy and apoptosis in birds lungs via PTEN/PI3K/AKT/mTOR. *Environ Toxicol*, 38(1):78-89. https://doi.org/10.1002/tox.23663

Lu HM, Zhang Y, Zhang X, et al., 2024. New insights into zinc alleviating renal toxicity of arsenic-exposed carp (*Cyprinus carpio*) through YAP-TFR/ROS signaling pathway. *Pestic Biochem Physiol*, 205:106153. https://doi.org/10.1016/j.pestbp.2024.106153

Lv M, Ma XB, Zhang KY, et al., 2023. The disruption of blood-brain barrier induced by long-term arsenic exposure is associated with the increase of MMP-9 and MMP-2: the characteristics are similar to those caused by senescence. *Chem Biol Interact*, 385:110743. https://doi.org/10.1016/j.cbi.2023.110743

Malewska-Kasprzak M, Skibińska M, Dmitrzak-Węglarz M, 2024. Alterations in neurotrophins in alcohol-addicted patients during alcohol withdrawal. *Brain Sci*, 14(6):583. https://doi.org/10.3390/brainsci14060583

Marlin MC, Li GP, 2015. Biogenesis and function of the NGF/TrkA signaling endosome. *Int Rev Cell Mol Biol*, 314:239-257. https://doi.org/10.1016/bs.ircmb.2014.10.002

Martorana F, Gaglio D, Bianco MR, et al., 2018. Differentiation by nerve growth factor (NGF) involves mechanisms of crosstalk between energy homeostasis and mitochondrial remodeling. *Cell Death Dis*, 9(3):391. https://doi.org/10.1038/s41419-018-0429-9

Mu MY, Zhao HJ, Wang Y, et al., 2019. Arsenic trioxide or/and copper sulfate co-exposure induce glandular stomach of chicken injury via destruction of the mitochondrial dynamics and activation of apoptosis as well as autophagy. *Ecotoxicol Environ Saf*, 185:109678. https://doi.org/10.1016/j.ecoenv.2019.109678

Olichon A, Baricault L, Gas N, et al., 2003. Loss of OPA1 perturbates the mitochondrial inner membrane structure and integrity, leading to cytochrome c release and apoptosis. *J Biol Chem*, 278(10):7743-7746. https://doi.org/10.1074/jbc.C200677200

Olson L, 1993. NGF and the treatment of Alzheimer's disease. *Exp Neurol*, 124(1):5-15. https://doi.org/10.1006/exnr.1993.1167

Peel HR, Balogun FO, Bowers CA, et al., 2022. Towards understanding factors affecting arsenic, chromium, and vanadium mobility in the subsurface. *Water*, 14(22):3687.

https://doi.org/10.3390/w14223687

Prakash C, Soni M, Kumar V, 2016. Mitochondrial oxidative stress and dysfunction in arsenic neurotoxicity: a review. *J Appl Toxicol*, 36(2):179-188. https://doi.org/10.1002/jat.3256

Qin LY, Xi SH, 2022. The role of mitochondrial fission proteins in mitochondrial dynamics in kidney disease. *Int J Mol Sci*, 23(23):14725. https://doi.org/10.3390/ijms232314725

Sánchez-Infantes D, Cereijo R, Sebastiani G, et al., 2018. Nerve growth factor levels in term human infants: relationship to prenatal growth and early postnatal feeding. *Int J Endocrinol*, 2018:7562702. https://doi.org/10.1155/2018/7562702

Sang QL, Sun DJ, Chen ZH, et al., 2018. NGF and PI3K/Akt signaling participate in the ventral motor neuronal protection of curcumin in sciatic nerve injury rat models. *Biomed Pharmacother*, 103:1146-1153. https://doi.org/10.1016/j.biopha.2018.04.116

Schmitt K, Grimm A, Dallmann R, et al., 2018. Circadian control of DRP1 activity regulates mitochondrial dynamics and bioenergetics. *Cell Metab*, 27(3):657-666.e5. https://doi.org/10.1016/j.cmet.2018.01.011

Sevak P, Pushkar B, 2024. Arsenic pollution cycle, toxicity and sustainable remediation technologies: a comprehensive review and bibliometric analysis. *J Environ Manage*, 349:119504. https://doi.org/10.1016/j.jenvman.2023.119504

Sung K, Ferrari LF, Yang WL, et al., 2018. Swedish nerve growth factor mutation (NGF^{R100W}) defines a role for TrkA and $p75^{NTR}$ in nociception. *J Neurosci*, 38(14):3394-3413. https://doi.org/10.1523/JNEUROSCI.1686-17.2018

Tan Z, Kang T, Zhang XL, et al., 2019. Nerve growth factor prevents arsenic-induced toxicity in PC12 cells through the AKT/GSK-3β/NFAT pathway. *J Cell Physiol*, 234(4):4726-4738. https://doi.org/10.1002/jcp.27255

Tolins M, Ruchirawat M, Landrigan P, 2014. The developmental neurotoxicity of arsenic: cognitive and behavioral consequences of early life exposure. *Ann Glob Health*, 80(4):303-314. https://doi.org/10.1016/j.aogh.2014.09.005

Tsai MS, Lin YC, Sun CK, et al., 2014. Up-regulation of nerve growth factor in cholestatic livers and its hepatoprotective role against oxidative stress. *PLoS One*, 9(11):e112113. https://doi.org/10.1371/journal.pone.0112113

Tuon L, Tramontin NS, Custódio I, et al., 2023. Serum biomarkers to mild cognitive deficits in children and adolescents. *Mol Neurobiol*, 60(12):7080-7087. https://doi.org/10.1007/s12035-023-03536-z

Wang X, Huang XY, Zhou L, et al., 2021. Association of arsenic exposure and cognitive impairment: a population-based cross-sectional study in China. *NeuroToxicology*, 82:100-107. https://doi.org/10.1016/j.neuro.2020.11.009

Wang XK, Michaelis EK, 2010. Selective neuronal vulnerability to oxidative stress in the brain. *Front Aging Neurosci*, 2:12. https://doi.org/10.3389/fnagi.2010.00012

Wang YZ, Wang YC, Liu W, et al., 2023. TIM-4 orchestrates mitochondrial homeostasis to promote lung cancer progression *via* ANXA2/PI3K/AKT/OPA1 axis. *Cell Death Dis*, 14(2):141. https://doi.org/10.1038/s41419-023-05678-3

Xing SP, Zhang CR, Guo HM, et al., 2024. Hydrologic changes induced by groundwater abstraction lead to arsenic mobilization in shallow aquifers. *J Hazard Mater*, 480:136133. https://doi.org/10.1016/j.jhazmat.2024.136133

Yan T, Zhang ZH, Li DQ, 2020. NGF receptors and PI3K/AKT pathway involved in glucose fluctuation-induced damage to neurons and α-lipoic acid treatment. *BMC Neurosci*, 21:38. https://doi.org/10.1186/s12868-020-00588-y

Yapa NMB, Lisnyak V, Reljic B, et al., 2021. Mitochondrial dynamics in health and disease. *FEBS Lett*, 595(8):1184-1204. https://doi.org/10.1002/1873-3468.14077

Ye FP, Wu L, Li H, et al., 2023. SIRT1/PGC-1α is involved in arsenic-induced male reproductive damage through mitochondrial dysfunction, which is blocked by the antioxidative effect of zinc. *Environ Pollut*, 320:121084. https://doi.org/10.1016/j.envpol.2023.121084

Supplementary information

Tables S1 and S2; Figs. S1 and S2